


# Surface solitonic charge distribution on 2D materials investigated using Kelvin probe force microscopy technique based on qplus atomic force microscopy

Rui Song(宋睿), Feng Hao(郝峰), Jie Yang(杨杰), Lifeng Yin(殷立峰), and Jian Shen(沈健)

**Citation :**Chin. Phys. B, 2025, 34 (**5**): 056802. DOI: 10.1088/1674-1056/adbee8
http://cpb.iphy.ac.cn; http://iopscience.iop.org/cpb

**What follows is a list of articles you may be interested in**

---

## Growth and characterization of Bi(110)/$CrTe_2$ heterostructures: Exploring interplay between magnetism and topology

Zhenyu Yuan(袁震宇), Fazhi Yang(杨发枝), Baiqing Lv(吕佰晴), Yaobo Huang(黄耀波), Tian Qian(钱天), Jinpeng Xu(徐金朋), and Hong Ding(丁洪)

Chin. Phys. B, 2024, 33 (**2**): 026802. DOI: 10.1088/1674-1056/ad082a

## Adsorption structure of macrocyclic energetic molecule DOATF on Au(111)

Xiao Chang(常霄), Li Huang(黄立), Yixuan Gao(高艺璇), Changjiang Yu(于长江), Yun Cao(曹云), Long Lv(吕龙), Xiao Lin(林晓), Shixuan Du(杜世萱), and Hong-Jun Gao(高鸿钧)

Chin. Phys. B, 2023, 32 (**9**): 096802. DOI: 10.1088/1674-1056/acda84

## Phase transition-induced superstructures of *β*-Sn films with atomic-scale thickness

Le Lei(雷乐), Feiyue Cao(曹飞跃), Shuya Xing(邢淑雅), Haoyu Dong(董皓宇), Jianfeng Guo(郭剑锋), Shangzhi Gu(顾尚志), Yanyan Geng(耿燕燕), Shuo Mi(米烁), Hanxiang Wu(吴翰翔), Fei Pang(庞斐), Rui Xu(许瑞), Wei Ji(季威), and Zhihai Cheng(程志海)

Chin. Phys. B, 2021, 30 (**9**): 096804. DOI: 10.1088/1674-1056/ac11e8

## Epitaxial growth of antimony nanofilms on HOPG and thermal desorption to control the film thickness

Shuya Xing(邢淑雅), Le Lei(雷乐), Haoyu Dong(董皓宇), Jianfeng Guo(郭剑峰), Feiyue Cao(曹飞跃), Shangzhi Gu(顾尚志), Sabir Hussain, Fei Pang(庞斐), Wei Ji(季威), Rui Xu(许瑞), Zhihai Cheng(程志海)

Chin. Phys. B, 2020, 29 (**9**): 096801. DOI: 10.1088/1674-1056/aba27c

## Triphenylene adsorption on Cu(111) and relevant graphene self-assembly

Qiao-Yue Chen(陈乔悦), Jun-Jie Song(宋俊杰), Liwei Jing(井立威), Kaikai Huang(黄凯凯), Pimo He(何丕模), Hanjie Zhang(张寒洁)

Chin. Phys. B, 2020, 29 (**2**): 026801. DOI: 10.1088/1674-1056/ab6583

---

# Surface solitonic charge distribution on 2D materials investigated using Kelvin probe force microscopy technique based on qplus atomic force microscopy

Rui Song(宋睿)[2], Feng Hao(郝峰)[2], Jie Yang(杨杰)[2], Lifeng Yin(殷立峰)[1,2,3,4,†], and Jian Shen(沈健)[1,2,3,4,‡]

[1] *Shanghai Research Center for Quantum Sciences, Shanghai* 201315, *China*
[2] *State Key Laboratory of Surface Physics, Institute for Nanoelectronic Devices and Quantum Computing, and Department of Physics, Fudan University, Shanghai* 200438, *China*
[3] *Zhangjiang Fudan International Innovation Center, Fudan University, Shanghai* 201210, *China*
[4] *Collaborative Innovation Center of Advanced Microstructures, Nanjing* 210093, *China*

(Received 22 January 2025; revised manuscript received 27 February 2025; accepted manuscript online 11 March 2025)

Recently, charged solitons have been found in a two-dimensional $CoCl_2$/HOPG system, whose microscopic nature remains to be elusive. In this work, we investigate the charged solitons in monolayer $CoCl_2$ using scanning tunneling microscopy (STM) and atomic force microscopy (AFM). Moreover, we study the electrical properties of the charged solitons at zero electric field by measuring local contact potential difference (LCPD) via Kelvin probe force microscopy (KPFM) using the $\Delta f(V)$ method. The compensation voltage corresponding to the vertex of the parabola is obtained by fitting the quadratic relationship between $\Delta f$ and sample bias. The results show that, without an external electric field, the solitons behave as negatively charged entities. Meanwhile, the LCPD mapping characterizes the spatial distribution of the potential at the charged solitons, which agrees well with those obtained from STM band bending measurements.

**Keywords:** scanning tunneling microscopy (STM), atomic force microscopy (AFM), Kelvin probe force microscopy (KPFM), cobalt dichloride

**PACS:** 68.37.Ef, 68.37.Ps, 07.79.Cz

**DOI:** 10.1088/1674-1056/adbee8 **CSTR:** 32038.14.CPB.adbee8

## 1. Introduction

Recent research on the cobalt dichloride ($CoCl_2$) monolayer, a two-dimensional transition metal dichalcogenide (TMD) material grown on highly oriented pyrolytic graphite (HOPG), has revealed the formation of local charged solitons. These solitons are the result of cooperative charge–lattice deformations confined in the unit-cell scale. In the $CoCl_2$/HOPG system, charged solitons can be both electrically and positionally manipulated using the STM tip.[1–3] Additionally, the electrical polarity of these solitons can be controlled by the electric field applied via the STM tip.[3] Through band structure characterization, our previous study observes an antiparallel band bending effect, where the conduction or valence band bends upward under positive bias and downward under negative bias, respectively.[3] This finding is supported by nc-AFM measurements, which reveal paraelectric dipole characteristics of the solitons.[3] However, STM provides only an indirect method for determining the electrostatic potential by probing the band positions,[4–6] which can be easily influenced by factors such as defects,[7] band tailing effects[8] and so on. In contrast, the nc-AFM based KPFM technique can directly image the electrostatic potential distribution in real space, offering a more intuitive and accurate method for potential measurement.[9,10] In this study, we present a detailed investigation of the spatial distribution of electrostatic potential at the charged solitons in the $CoCl_2$/HOPG system using both STM and KPFM techniques.

STM and nc-AFM are both powerful methods to investigate sample surface in real space. Nc-AFM can achieve higher spatial resolution with suitable functionalized tip apex.[11–13] Compared to STM, nc-AFM-based KPFM technique has obvious advantages in electrostatic potential detection.[14] Nc-AFM based KPFM measurement usually operates in $\Delta f(V)$ spectroscopy mode, where frequency shift ($\Delta f$) is recorded as a function of sample bias. When electrostatic force caused by LCPD is compensated by sample bias, interaction force gradient between tip apex and sample is minimized.[15] If the electrostatic potential is not homogeneous over the interface, the bias required to compensate local contact potential varies in space. Recording the compensating voltage variation constructs the surface potential map (LCPD mapping), which also represents the electrostatic force distribution. The KPFM technique based on nc-AFM has been widely used in the measurement of dipole orientations of adsorbed molecules on metal surfaces.[10] Depending on the extraordinary sensitivity of LCPD, the KPFM technique can even distinguish the

†Corresponding author. E-mail: lifengyin@fudan.edu.cn
‡Corresponding author. E-mail: shenj5494@fudan.edu.cn

© 2025 Chinese Physical Society and IOP Publishing Ltd. All rights, including for text and data mining, AI training, and similar technologies, are reserved.

charging and discharging processes of a single electron.[16] The KPFM technique plays an important role in condensed matter physics research.[17,18]

## 2. Methods

### 2.1. Sample preparation

Monolayer $CoCl_2$ samples were grown on cleaved HOPG substrate by MBE method using a Knudsen cell (K-cell) source at a base pressure of about $1.0 \times 10^{-10}$ mbar. The source temperature was set to 340 °C to evaporate $CoCl_2$, and the substrate was kept at 42 °C during the growth procedure. The whole growth process lasted 1.5 hours. Reflective high-energy electron diffraction (RHEED) was performed to monitor the growth process. After growth, samples were annealed at 110 °C for one hour before being transferred to the chamber where STM and nc-AFM measurements were performed by a home-built UHV suitcase (base pressure lower than $5.0\times10^{-11}$ mbar).

### 2.2. STM/AFM measurements

All experimental data were acquired by a home-built cryogen-free low temperature STM/nc-AFM system with a base pressure lower than $5.0\times10^{-11}$ mbar, operating at a temperature of 5.4 K. The STM tips were calibrated on a Au (111) surface by checking the surface states around −0.5 V. Scanning tunneling spectroscopy (STS) was obtained using the lock-in amplifier technique with a modulation frequency of 984.58 Hz and a modulation amplitude of 40 mV.

Home-built qplus sensor was used to perform nc-AFM measurement. AFM tips (tungsten wire, 0.025 mm) were also calibrated on a Au (111) surface by checking if the frequency shift was suitable at a specific tunnelling parameter. The frequency shift of each tip was processed to about −1 Hz to −2 Hz at 0.1 V and 10 pA tunneling parameters. The resonant frequency of the tuning fork is $f_0 = 29013$ Hz. The stiffness is $k = 1800$ N/m, and the $Q$ factor is 78821. Nc-AFM imaging and KPFM mapping with qplus sensor were performed at frequency modulation mode with an oscillation amplitude of 100 pm.

## 3. Result and discussion

Figure 1(b) shows the side view atomic structure of 1T phase $CoCl_2$. Bulk $CoCl_2$ is a vdW material. In each vdW layer, there is a sandwich structure consisting of a Co sub-layer between two Cl sub-layers. All $Co^{2+}$ ions are arranged in a triangular lattice (Fig. 1(a)). Each $Co^{2+}$ ion and six nearest neighbor $Cl^-$ ions form an octahedral structure. The large area STM topography is shown in Fig. 1(c), where high quality monolayer $CoCl_2$ islands can be seen. Consistent with our previous studies, randomly distributed 'dark spots' exist on the island at high bias voltage (1 V, Fig. 1(d)), while a complete atomic lattice is clearly visible at low bias voltage (−0.1 V, Fig. 1(e)). Unlike static defects, these solitons can be easily written, manipulated, and erased by the tip.[1–3] Moiré pattern can also be clearly observed. High-resolution nc-AFM image of the same region (Fig. 1(f))

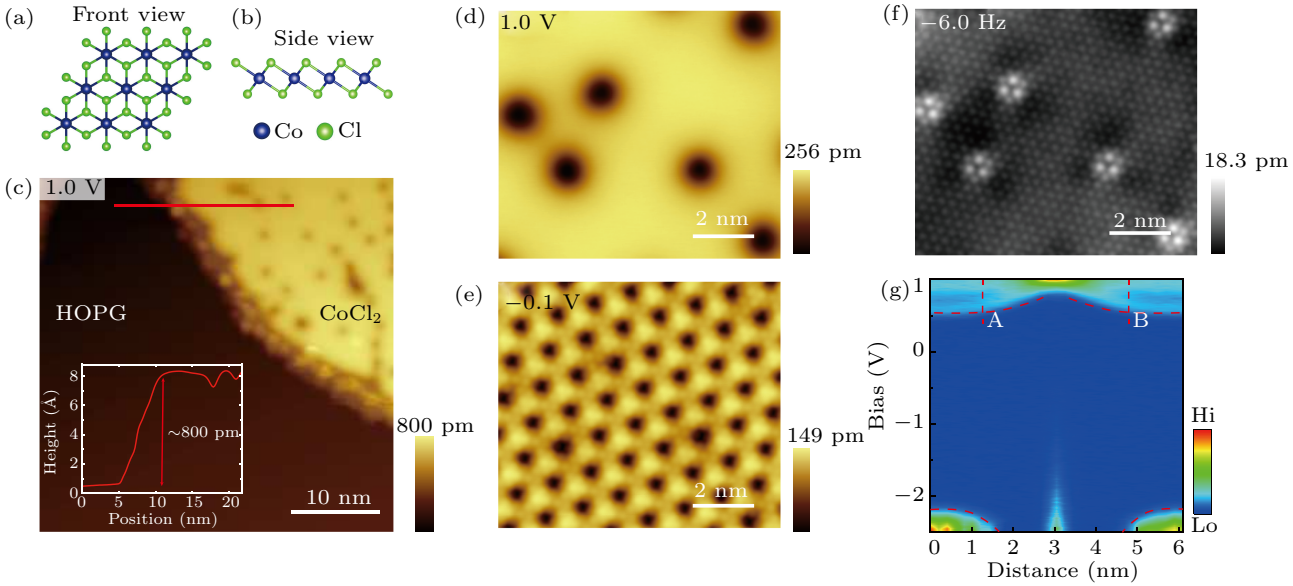



**Fig. 1.** STM, AFM topography and band bending effect of solitons measured on $CoCl_2$/HOPG system. (a), (b) Front and side views of crystal structure of single layer $CoCl_2$. (c) Large scale STM topography of monolayer $CoCl_2$ grown on HOPG, illustrating high quality epitaxial film. The inset shows terrace height of about 800 pm. ($V_s = 1.0$ V, $I_t = 10$ pA) (d)–(f) STM topography in different tunnelling condition and nc-AFM atomic resolution in exactly the same area. The STM topography shows an isolated distribution of solitons at large sample bias ($V_s = 1.0$ V, $I_t = 40$ pA) and a complete atomic lattice with moiré pattern at small sample bias ($V_s = -0.1$ V, $I_t = 40$ pA). AFM image shows that each soliton corresponds to a trimer structure. STM and AFM atomic resolution images show a lattice constant of ∼ 3.6 Å ($V_s = 0$ V, $\Delta f = -6.0$ Hz, $A = 100$ pm). (g) 2D $\mathrm{d}I/\mathrm{d}V$ plot cross soliton along the dash white line in Fig. 2(a) indicates antiparallel band bending effect. $d_{AB}$ is about 3.5 nm, which means the extent of impact of single soliton is about 3.5 nm. Spectroscopic condition: $V_s = 1.0$ V, $I_t = 60$ pA.

shows that each 'dark spot' position corresponds to a trimeric structure orientated in the same direction. By employing nc-AFM force curve analysis which is able to serve as fingerprints for identification of chemical elements, we have ascertained that the soliton trimer exhibits a Morse potential consistent with other Cl ions.[19–22] Height difference of these trimers with respect to the trivial position ranged from a few picometers to several tens of picometers depends on the sample bias.[3]

The most intriguing phenomenon in the $CoCl_2$/HOPG system is the appearance of the 'dark spots' at large bias voltages, which we refer to as solitons.[1–3] In our previous work,[3] we conducted $\mathrm{d}I/\mathrm{d}V$ measurements on and away from the soliton, revealing a tunnelling mechanism difference, i.e., tunnelling to HOPG occurs on soliton site and tunnelling to $CoCl_2$ occurs away from the soliton site, depending on the comparison of local band edge and tunneling bias. $\mathrm{d}I/\mathrm{d}V$ line profile measurements cross the soliton reveal antiparallel band bending at positive and negative sample bias. At large positive bias, the influence of the soliton extends over a region of approximately 3.5 nm (as indicated by $d_{\mathrm{AB}}$ in Fig. 1(g), $\sim 3.5$ nm).

However, STM is unable to directly access the charge polarity of soliton in real space, whereas KPFM measurements based on nc-AFM can achieve this purpose by measuring LCPD.[23] The LCPD measurements are affected by many factors, such as the tip shape, tip chemical components and tip–sample distance. To control the tip shape effect, the tips we use for KPFM measurements are carefully calibrated on Au (111) single crystals before imaging the sample. In this case, tips can be considered as clean metal tips, whose dipole effect can be ignored,[23] and also do not have irregular shapes that are affected by impurities. (After impurities are adsorbed onto the tip, solitons in AFM imaging will not be a perfect trimer shape, through which we can confirm the tip shape.) To control the effect of tip–sample distance, we experimentally characterize the relationship between the LCPD and $\Delta z$ (tip–sample distance). Figure 2(a) is the STM topography, where we measured the $\Delta f(V)$ spectroscopies at a series of continuously varying tip–sample distances from the point at the center (red triangle mark) of the soliton and the point at the bottom left corner (blue square mark) of the image. For each spectral line (Fig. 2(b)), the horizontal coordinate of the parabolic vertex is LCPD (compensation voltage, $V_{\mathrm{LCPD}}$), and the vertical coordinate is the sum of the remaining force gradients excluding the effect of bias voltage (denoted as $\Delta f^*$). Figure 2(c) plots the LCPD as a function of the tip–sample distances. We define the tunnelling height corresponding to the setpoint of 1 V, 10 pA as $\Delta z = 0$. Starting from the initial point, negative $\Delta z$ means that the tip is closer to the sample, while a positive $\Delta z$ means the tip is further away. At all tip–sample distances, we observe that the LCPD at the soliton center is higher than that at the soliton free area. As the tip–sample distance increases, LCPD at the soliton center gradually decreases, while the LCPD at the soliton free area gradually increases but will never exceed that at the soliton center. We find that the LCPD at both locations change very slowly after $\Delta z$ is higher than 400 pm, maintaining a LCPD difference of about 40 mV–70 mV. At tip–sample distances less than 400 pm, the LCPD difference between the soliton center and the soliton free area increases as the tip approaches the sample. This phenomenon can be explained by the averaging effect.[24] As an example, for the soliton center position, when the tip is very close to the sample, the influence of surrounding soliton free region on the LCPD measurement is small. When the tip–sample distance increases, the surrounding soliton free region shifts the LCPD at the center of the soliton towards a smaller value. Similarly, the result of the averaging effect on the soliton free area is to shift the LCPD towards a larger value. The difference of LCPD between the two sites will gradually decrease when we lift the tip away, which perfectly fits our experimental data.

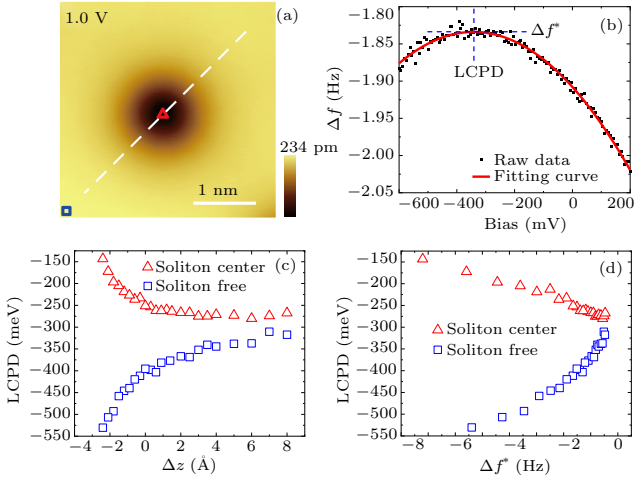



**Fig. 2.** Influence of tip–sample distance ($\Delta z$) on LCPD. (a) Constant-current STM image ($V_{\mathrm{s}} = 1.0$ V, $I_{\mathrm{t}} = 10$ pA). $\mathrm{d}I/\mathrm{d}V$ plot is performed along dash line direction from bottom left corner to top right corner. It is important to note that the dash line only marks the $\mathrm{d}I/\mathrm{d}V$ plot direction, the length of the dash line is not equal to the actual $\mathrm{d}I/\mathrm{d}V$ plot length. (b) $\Delta f(V)$ curve measured at blue square point in (a). This curve is fitted by means of a parabola, where the horizontal coordinate is LCPD (the compensating voltage), and the vertical coordinate is defined as $\Delta f^*$, which represents the sum of the gradients of the other forces that are not affected by the sample bias. (c) LCPD measured at different tip–sample distances ($\Delta z$) and positions with feedback loop off. Blue squares and red triangles represent soliton free and soliton center, respectively. The $\Delta f(V)$ curves were measured for each tip height and the LCPD was obtained by parabolic fitting. LCPD is shown as a function of $\Delta z$. (d) LCPD shown as a function of $\Delta f^*$, which means that the same LCPD contrast can be obtained using frequency modulation mode. The tip did not change in all of the above measurements.

For the LCPD mapping measurement modes of the $\Delta f(V)$ method, there are two options to choose from: constant height mode and frequency modulation mode (constant frequency mode). In constant height mode measurement, there is no need to set up a feedback loop for $\Delta f$. Therefore, this is the preferred mode for LCPD measurement.[25,26] However,

constant height measurement inevitably generates temperature drift during long and fine mapping measurements (about 6–10 hours), and the absolute height between tip and sample will change. The measurement results of LCPD are distance-dependent, so we have to consider the possibility of using frequency modulation mode to measure LCPD mapping. In Fig. 3(a), at −0.4 V scanning bias voltage, trimer (soliton position) is about 10 pm higher than the surrounding atoms which are considered as soliton free area in high sample bias. However, this height difference depends on the bias voltage, with the height difference being smaller at positive bias than at negative bias.[3] If the scanning bias voltage for LCPD mapping is set to a positive bias voltage (0.2 V, for example), and the $\Delta f(V)$ curves start scanning from the same value. In this case, the height difference of the tip as it scans over the trimer is only a few picometers. This implies that, during scanning in frequency modulation mode, the relative distance between the tip and the sample varies very little, which is comparable to, or even smaller than, the variation caused by temperature drift over a long period of mapping time. To verify this, we conducted a comparison between the constant frequency mode and constant height mode. With appropriate feedback loop settings, both modes produced identical experimental results. This conclusion is further supported by Fig. 2(d), where the contrast of LCPD mapping in the constant frequency mode is consistent with that in constant height mode. Therefore, for long-duration and fine spectroscopy measurements, we ultimately chose the frequency modulation mode to acquire the LCPD mapping data.

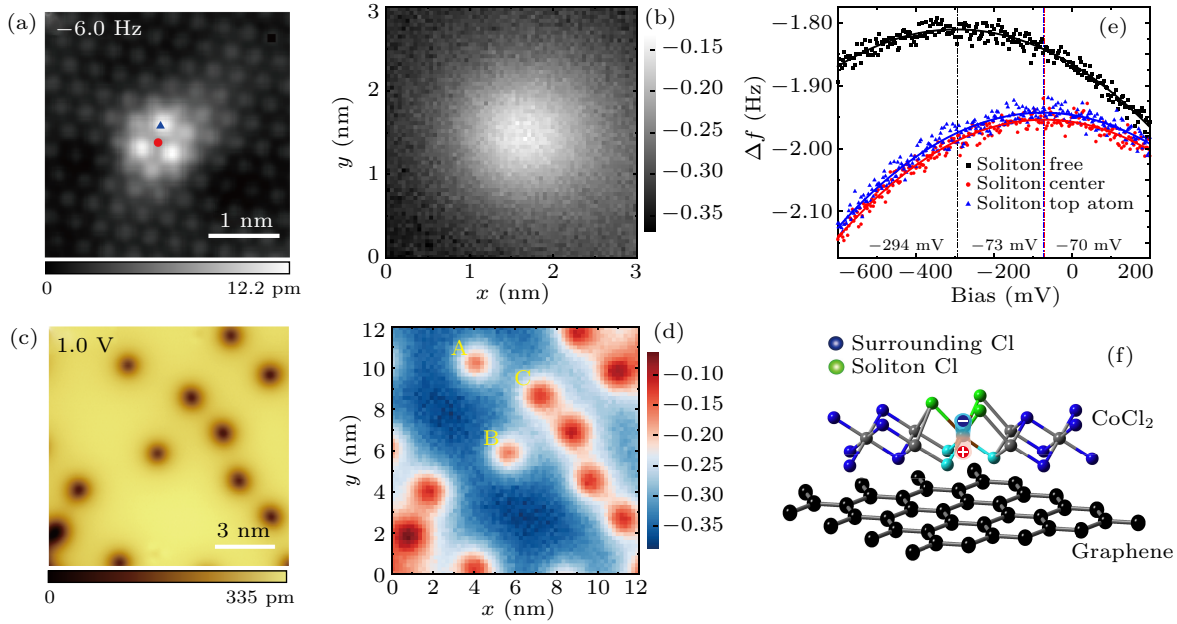



**Fig. 3.** LCPD mapping measurements for single soliton and multiple solitons. (a) Frequency modulation nc-AFM image of a single soliton ($V_s = -0.4$ V, $\Delta f = -6.0$ Hz, $A = 100$ pm). (b) LCPD mapping of a single soliton shown in (a). (c) Constant-current STM image of several solitons ($V_s = 1.0$ V, $I_t = 10$ pA). (d) LCPD mapping of multiple solitons shown in (c). The distance between points A and C is 3.5 nm. The distance between B and C is 3.2 nm. (e) $\Delta f(V)$ curves measured at different points marked in (a). Black square represents soliton free region, blue triangle represents soliton trimer vertex atom, and red circle represents soliton center. (f) A schematic illustrating the dipole orientation (pointing from vacuum to the sample).

Figure 3(b) presents the experimental results of LCPD mapping obtained using frequency modulation mode measurements. We perform LCPD mapping of a single soliton as well as multiple solitons. Before starting the mapping measurement, single $\Delta f(V)$ spectra at soliton and soliton free area are firstly measured. These measurements are conducted with the feedback loop off and positioned at the corresponding points in Fig. 3(a) (red circle, blue triangle and black square). Owing to the ultra-high atomic resolution of nc-AFM, we are able to finely measure the difference between the compensation voltages of each atom in the trimer compared to the surrounding atoms in the trivial positions, as shown in Fig. 3(e). We observe that the compensation voltage for the top atom in the trimer and trimer center is −73 mV and −70 mV, respectively, while the compensation voltage in the trivial position is −294 mV. This LCPD shift indicates that a smaller negative voltage (absolute value) is required to compensate the LCPD at the soliton position, whereas a larger negative voltage in absolute value is needed at the trivial positions. The frequency modulation LCPD mapping setpoint is $\Delta f = -2$ Hz. In addition to the LCPD shift between soliton center and soliton free area, we also find that a larger attractive force is always observed at the soliton center compared to the soliton free region. This is consistent with the nc-AFM images, where the tip needs to be retracted at the soliton center to maintain the same $\Delta f$ as in the surrounding region. Immediately after the completion of the single-point spectroscopy measurements, we proceeded with the LCPD mapping by dividing the ex-

perimental area into a grid and performing single-point $\Delta f(V)$ spectroscopy at each pixel. The spatial distribution of the compensating voltages was then fitted to generate the LCPD mapping. The LCPD mapping confirmed that the LCPD at the soliton position is significantly higher than that at the soliton-free area, which means that the soliton behaves as a negatively charged entity without external electric field. This, combined with the band bending observed in the opposite direction, implies the presence of a dipole with its orientation pointing from the vacuum towards the sample.[27] The dipole distributed in this direction locally raises the work function, which means that the sample must be biased towards a more positive direction to compensate for the effect of the negative charge here.[16,28,29] It is worth noting that the LCPD measured by KPFM does not simply represent the absolute strength of the dipole, while the direction of LCPD shift depends and only depends on the direction of the dipole at that particular position.

After completing the measurements on single solitons, we also perform LCPD mapping on regions where multiple solitons coexist. The results, as shown in Fig. 3(d), reveal that the LCPD mapping for multiple solitons does not differ from that of a single soliton. At all soliton locations, we observe localized LCPD elevations. Additionally, we find that if the center-to-center distance between different solitons exceeds 3.5 nm (e.g., soliton A and soliton C, $d_{\mathrm{AC}} = 3.5$ nm), their potential distributions do not overlap. However, when the center-to-center distance between two solitons is less than 3.5 nm (e.g., soliton B and soliton C, $d_{\mathrm{BC}} = 3.2$ nm), their potential distributions clearly overlap, forming an elevated potential plateau. This observation aligns with the conclusion from the STM band bending measurements, where the dipole-induced bending effect on the band is almost negligible outside a circle with a radius of 3.5 nm centered at the soliton ($d_{\mathrm{AB}}$ in Fig. 1(g) is 3.5 nm).

## 4. Conclusion and perspectives

We used STM and nc-AFM to characterize the atomic structure and charged properties of the solitons on monolayer $CoCl_2$ grown on HOPG. In STM images, the charged solitons appear as circular depressions forming dark spots at high sample bias, and a complete atomic lattice at low sample bias. Combining with STM band bending experimental results, the LCPD shifts obtained from nc-AFM based KPFM measurements show that the negatively charged soliton could be a single dipole whose direction points from vacuum to the sample. Its potential is distributed in a circular area with a radius of about 3.5 nm centered on the soliton center, which is consistent with the range of influence length obtained by measuring the band bending effect in STM.

Our work has successfully elucidated the polarization orientation of solitons within the $CoCl_2$/HOPG system at zero electric field with the KPFM technique. This discovery advances our comprehension of the behavior of charged solitons in this particular system. Looking ahead, one can perform experiments involving the reversal of electric fields to explore the intriguing outcomes that LCPD may exhibit following the reversal of soliton polarization. Since scanning voltages are required during KPFM measurements, it is difficult to obtain LCPD mapping with a constant polarized electric field. It is hoped that $\mathrm{d}I/\mathrm{d}z$ (proportional to work function) mapping[30,31] at different voltages will solve this difficulty.

## Acknowledgements

Project supported by the National Key Research and Development Program of China (Grant Nos. 2022YFA1403300 and 2019YFA0308404), the National Natural Science Foundation of China (Grant Nos. 11427902, 11991060, 12074075, 12474165, 12274084, and 12241402), Shanghai Municipal Science and Technology Major Project (Grant No. 2019SHZDZX01), Shanghai Municipal Natural Science Foundation (Grant No. 22ZR1407400), Innovation Program for Quantum Science and Technology (Grant No. 2024ZD0300104), Innovation Program of Shanghai Municipal Education Commission (Grant No. 2023ZKZD03), Science and Technology Commission of Shanghai Municipality (Grant No. 20JC1415900), and China Postdoctoral Science Foundation (Grant No. KLH1512149).

## References

[1] Liu H, Wang A, Zhang P, Ma C, Chen C, Liu Z, Zhang Y Q, Feng B, Cheng P, Zhao J, Chen L and Wu K 2023 *Nat. Commun.* **14** 3690
[2] Cai M, Miao M P, Liang Y, Jiang Z, Liu Z Y, Zhang W H, Liao X, Zhu L F, West D, Zhang S and Fu Y S 2023 *Nat. Commun.* **14** 3691
[3] Hao F, Song R, Yang J, Shen J, Ernst A, Yin L, Wang Z and Gao C 2024 *Nano Lett.* **24** 14042
[4] Zhu Z, Chang T R, Huang C Y, Pan H, Nie X A, Wang X Z, Jin Z T, Xu S Y, Huang S M, Guan D D, Wang S, Li Y Y, Liu C, Qian D, Ku W, Song F, Lin H, Zheng H and Jia J F 2018 *Nat. Commun.* **9** 4153
[5] Crommie M F, Lutz C P and Eigler D M 1993 *Nature* **363** 524
[6] Rutter G M, Crain J N, Guisinger N P, Li T, First P N and Stroscio J A 2007 *Science* **317** 219
[7] Garnica M, Otrokov M M, Aguilar P C, Klimovskikh I I, Estyunin D, Aliev Z S, Amiraslanov I R, Abdullayev N A, Zverev V N, Babanly M B, Mamedov N T, Shikin A M, Arnau A, de Parga A L V, Chulkov E V and Miranda R 2022 *npj Quantum Materials* **7** 7
[8] Sutter-Fella C M, Miller D W, Ngo Q P, Roe E T, Toma F M, Sharp I D, Lonergan M C and Javey A 2017 *ACS Energy Letters* **2** 709
[9] Melitz W, Shen J, Kummel A C and Lee S 2011 *Surface Science Reports* **66** 1
[10] Mohn F, Gross L, Moll N and Meyer G 2012 *Nat. Nanotechnol.* **7** 227
[11] Gross L, Mohn F, Moll N, Liljeroth P and Meyer T 2009 *Science* **325** 1110
[12] Huang L, Kong X, Zheng Q, Xing Y, Chen H, Li Y, Hu Z, Zhu S, Qiao J, Zhang Y Y, Cheng H, Cheng Z, Qiu X, Liu E, Lei H, Lin X, Wang Z, Yang H, Ji W and Gao H J 2023 *Nat. Commun.* **14** 5230
[13] Chen P, Fan D, Selloni A, Carter E A, Arnold C B, Zhang Y, Gross A S, Chelikowsky J R and Yao N 2023 *Nat. Commun.* **14** 1460
[14] Albrecht F, Repp J, Fleischmann M, Scheer M, Ondráček M and Jelínek P 2015 *Phys. Rev. Lett.* **115** 076101

[15] Gou J, Bai H, Zhang X, Huang Y L, Duan S, Ariando A, Yang S A, Chen L, Lu Y and Wee A S T 2023 *Nature* **617** 67
[16] Gross L, Mohn F, Liljeroth P, Repp J, Giessibl F J and Meyer G 2009 *Science* **324** 1428
[17] Li H, Wang G B, Yang J Y, Zhang Z S, Deng J and Du S X 2023 *Chin. Phys. Lett.* **40** 128101
[18] Luo Y, Su W T, Zhang J J, Chen F, Wu K, Zeng Y J and Lu H W 2023 *Chin. Phys. B* **32** 117801
[19] Sugimoto Y, Pou P, Abe M, Jelinek P, Pérez R, Morita S and Custance Ó 2007 *Nature* **446** 64
[20] Sugimoto Y, Pou P, Custance Ó, Jelinek P, Morita S, Pérez R and Abe M 2006 *Phys. Rev. B* **73** 205329
[21] Morse P M 1929 *Phys. Rev.* **34** 57
[22] Sugimoto Y, Namikawa T, Abe M and Morita S 2009 *Appl. Phys. Lett.* **94** 023108
[23] Ichii T, Fukuma T, Yoda T, Kobayashi L, Matsushige K and Yamada H 2010 *J. Appl. Phys.* **107** 024315
[24] Yuan B, Chen P, Zhang J, Cheng Z, Qiu X and Wang C 2013 *Chinese Science Bulletin* **58** 3630
[25] Krull C, Castelli M, Hapala P, Kumar D, Tadich A, Capsoni M, Edmonds M T, Hellerstedt K, Burke S A, Jelinek P and Schiffrin A 2018 *Nat. Commun.* **9** 3211
[26] Wang Y S, Li X, Yang Q X, Shen Q, He Y, Zhang Y J and Wang Y F 2023 *Fundamental Research*
[27] Telychko M, Edalatmanesh S, Leng K, Abdelwahab I, Guo N, Zhang C, Mendieta-Moreno J I, Nachtigall M, Li J, Loh K P, Jelínek P and Lu J 2022 *Sci. Adv.* **8** eabj0395
[28] Ikeda M, Koide N, Han L, Sasahara A and Onishi H 2008 *The Journal of Physical Chemistry C* **112** 6961
[29] Schuler B, Liu S X, Geng Y, Decurtins S, Meyer G and Gross L 2014 *Nano Lett.* **14** 3342
[30] Castenmiller C, van Bremen R, Sotthewes K, Siekman M H and Zandvliet H J W 2018 *AIP Adv.* **8** 075013
[31] Mishra R and Moheimani S O R 2025 *Rev. Sci. Instrum.* **96** 14